Lab on a Chip

Accepted Manuscript

ROYAL SOCIETY OF CHEMISTRY

www.rsc.org/loc

Journal Name

Lab on a Chip

Dynamic Article Links►

Cite this: DOI: 10.1039/c0xx00000x

www.rsc.org/xxxxxx

ARTICLE TYPE

Optofluidic holographic microscopy with custom Field of View by a linear array detector

V. Bianco,[a] M. Paturzo,[a,*] V. Marchesano,[a] I. Gallotta,[b] E. Di Schiavi[b] and P. Ferraro[a]

Received (in XXX, XXX) XthXXXXXXXXX 20XX, Accepted Xth XXXXXXXXX 20XX

DOI: 10.1039/b000000x

Simple and effective imaging strategies are of utmost interest for application at lab-on-chip scale. In fact, the majority of diagnostics tools are still image-based approaches for medical as well as biotechnology studies. Having on board chip a compact but powerful imaging apparatus with multiple imaging capabilities such as 3D dynamic focusing along the optical axis, unlimited field-of-view and twice outputs, namely intensity and quantitative phase-contrast maps on biological objects, is of extreme importance for the next generation of Lab-on-a-Chip (LoC) devices. Here we present a coherent 3D microscopy approach in holographic modality that looks specifically suitable for studying biological samples while they are simply flowing along microfluidic paths. The LoC device is equipped with a compact linear array detector for capturing and synthesize a new conceptual type of digital hologram in the space-time domain, named here Space-Time Digital Hologram (STDH). Reported results show that the method is a promising diagnostic tool for optofluidic investigations of biological specimens.

1. Introduction

Optical imaging of biological samples in microfluidic platforms is a highly demanded capability in all fields of biomedical research, biomaterials engineering and global healthcare for point-of-care diagnostics [1-6]. The development of Lab-on-a-Chip devices has recently experienced an impressive growth with the design of compact and low cost systems for biological samples counting, sorting and manipulation, e.g. by optical trapping [7-16]. In this framework, compact, and reliable imaging systems are highly demanded to provide 3D information about samples flowing in microfluidic channels. At this purpose, label-free techniques are preferred whenever invasive sample pre-treatment has to be avoided [17-18]. Moreover, full-field imaging capabilities are strongly required to provide quantitative phase-contrast information for rapid diagnostics purposes. Besides, the design of simple imaging schemes yielding high throughput are pursued with the final goal to fabricate a compact device with all the imaging functionalities embedded in a single small chip. Label-free phase retrieval techniques allowing in-vivo experiments onboard microfluidic platforms have been proven relying on Phase-Shifting Interferometry (PSI) [19-23], tomography [24-26], Digital Holography microscopy [9,10,12,16,17,27,28] and the more recently assessed Fourier Ptychographic Microscopy [29] (FPM). Methods employing low coherence light sources yield high Signal-to-Noise Ratio (SNR) images, being immune to coherent speckle artifacts, but multiple acquisitions, a complex set-up, and/or iterative phase retrieval algorithms have to be adopted to provide flexible focusing capabilities and to get quantitative phase-contrast maps.

Great effort has been spent to exploit the object motion along the chip for imaging purposes. A groundbreaking novelty in this direction is represented by the Optofluidic Microscope (OFM) [30], which detects the signal transmitted through skewed apertures realized in one of the microfluidic channel walls. Thus, by adjusting the aperture spacing it is possible to tune the achievable spatial resolution. However, in OFM the sample is bounded to stay in close contact with the apertures, which impairs the imaging of flowing objects in relatively deep channel and liquid volume. Furthermore, no phase information as well as flexible refocusing are achievable. A lensless microfluidic imaging system was also designed recently, where the samples are imaged simultaneously by three different wavelengths diode laser sources for recording the resulting near-field diffraction patterns as inputs of a phase-retrieval algorithm [31,32]. Although phase-contrast mapping and flexible refocusing were demonstrated, such a system does not fully exploit the intrinsic sample motion and the need to record a near field diffraction pattern limits the system to lensless recordings, in turn resulting in a limited magnification obtainable. Another interesting lens-based approach which moves a step toward the integration of the imaging functionalities inside the chip was reported [33,34], where the diffraction from a slit is exploited to build a stack of images with angular diversity for tomography purposes, yielding re-focusable amplitude and differential phase contrast images of flowing samples. On the other hand, Lensless Object Scanning Holography (LOSH) as well as synthetic aperture holography [35-39] adopt a shift of the detector to generate a synthetic hologram with remarkably enhanced reconstruction quality in terms of resolution, Field of View (FoV), and SNR. However, multiple holograms have to be properly combined in the Fourier

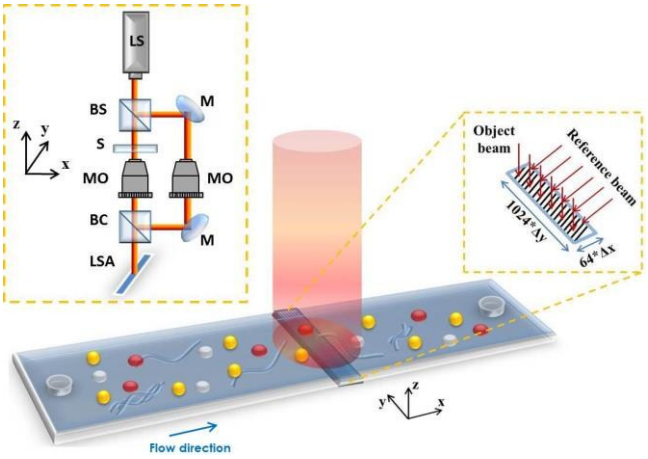

Fig. 1 Experimental set-up for microfluidic Space-Time Scanning Interferometry (μSTSI). Thanks to the intrinsic scanning due to the sample flow it is possible to build up, with a compact Linear Sensor Array (LSA), a Space-Time Digital Hologram (STDH) providing phase-contrast mapping with unlimited FoV in the flow direction. LS: Laser source. BS: Beam Splitter. BC: Beam Combiner. S: sample. MO: Microscope Objective. M: Mirror

domain and the method performance is severely dependent on the object spectrum shape. A remarkable way to exploit the object motion along the channel is reported in [40,41], where data capture is performed with a compact on chip set-up and the object sub-pixel shifts are exploited to record multiple holograms representing the whole specimen inside the system FoV, so that a pixel super-resolution algorithm [40,42] can be applied to yield a four-fold resolution gain. As in common 2D sensor-based approaches, a trade-off exists between the chosen magnification and the obtainable FoV.

A novel concept recording modality has been recently proposed, named Space Time Scanning Interferometry (STSI) [43], which exploits the object movement to generate synthetic interferograms with the desired phase shift between them and PSI has been realized adopting well-known algorithms [19-23]. Noteworthy, a small subset of detecting elements is proved to be sufficient to accomplish the PSI task [43]. In particular, in focus recordings were carried out with complex shaped objects (the object spectrum shape is not an issue in STSI) and the object motion was provided by a translational stage.

Here we first show the application of STSI to bio-microfluidics (herein referred to as μSTSI) with the aim to demonstrate that phase-contrast mapping with unlimited FoV along the flow direction is obtainable with a compact Linear Sensor Array (LSA) easy to be embedded in a LoC platform. In fact, such technique looks particularly suited in all the cases where the object shift is an intrinsic feature of the system, such as in microfluidics. The μSTSI method is briefly summarized in the following section, where the direct synthesis of space-time interferograms is described along with the processing steps required to obtain enlarged FoV phase-contrast maps by a LSA.

Besides, we demonstrate 3D imaging capability through the direct synthesis of what we named as Space-Time Digital Hologram (STDH), still maintaining all the advantageous capabilities of Digital Holography (DH) for refocusing biological samples flowing inside the chip at different image planes along the optical axis. We prove that the trade-off between the desired magnification and the FoV can be overcome by STDH, as occurs in other systems [30-34], but providing fast-unlimited FoV phase-contrast mapping without the need for hologram stitching. The synthesis and numerical propagation of a STDH is proved, which can be accomplished with just one line of the LSA, moving an important step toward the integration of quantitative, label-free, 3D imaging functions onboard chip for high throughput microfluidic applications.

2. Working principle

In this section, we briefly summarize the process allowing the direct synthesis of space-time holograms captured with compact linear sensor arrays and providing unlimited FoV in the flow direction. Let

$$H_1(x,y,t_1),...,H_K(x,y,t_K) \qquad (1)$$

be the time sequence of recorded holograms in the acquisition plane (x,y), each one coding, as amplitude and phase modulation of the interference fringes, the whole complex 3D information of the objects flowing along the microfluidic channel in the x direction. For the sake of clarity we will herein consider the general case of acquisitions with a 2D square sensor with MxN pixels, although a linear array made of Mx1 pixel or a rectangular one made of MxL (L<<N) pixel, displaced orthogonally to the flow direction could be fruitfully used for the scope. If just one line $x=x_0$ is selected from the stack in Eq. (1), it is possible to extract the set of vectors:

$$\begin{aligned} \mathbf{h}_{01} &= H_1(x_0,y,t_1) \\ \mathbf{h}_{02} &= H_2(x_0,y,t_2) \\ &\vdots \\ \mathbf{h}_{0K} &= H_K(x_0,y,t_K) \end{aligned} \qquad (2)$$

that can be rearranged in a matrix $H_{S0}(y,t)$ constituting a synthetic space-time hologram containing the whole complex information about the acquired time sequence. This is still coded as amplitude and phase modulation of interference fringes. In particular, if straight and parallel fringes are acquired with spatial pitch *p*, the synthesis process produces an interferogram with equally spaced fringes, always parallel to the flow direction and with spacing $p_{synth}=p/\cos\gamma$, set by the angle between the fringes and the x axis, γ. Interestingly, adding vectors so built to the matrix H_{S0} results in a FoV enlargement which is in principle unlimited in the x direction. If a linear array is employed, unlimited FoV DH microscopy can be achieved by numerical propagation of the matrix $H_{S0}(y,t)$, e.g. using the Fresnel transform or the Angular Spectrum method. In this case it is convenient to select the angle γ in order to minimize p_{synth}, thus providing a proper sampling of the objects by horizontal fringes. If a rectangular MxL (L<<N) sensor is available, each selected line $x=x_i$, i=1,…,L, can be in principle exploited to build a synthetic interferogram.

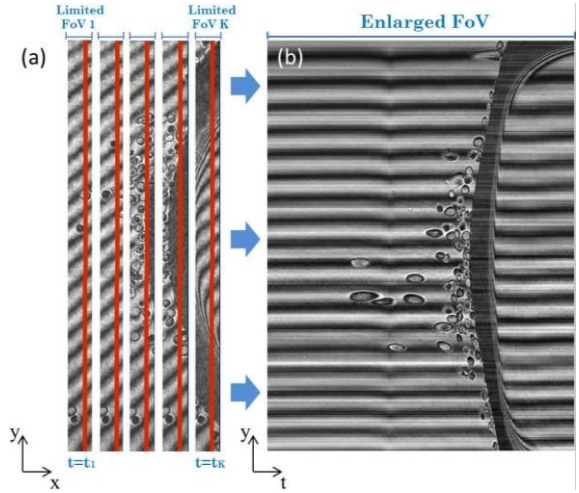

Fig. 2 μSTSI synthesis. Fibroblasts placed inside the channel are accelerated by an air bubble (Supplementary Movie 1). Figure shows the process of synthesis of a space-time interferogram with enlarged FoV (b) starting from Limited FoV recordings (a). The red solid lines in (a) show the detection gate, i.e. the line used to build up the interferogram in Fig. 2(b).

In this case we end up with the matrices stack

$$\Sigma=\begin{bmatrix} H_{s1}(y,t) \\ H_{s2}(y,t) \\ \vdots \\ H_{sL}(y,t) \end{bmatrix} \qquad (3)$$

resulting of interest as a different information can be extracted from each element of Σ. In particular, an intrinsic phase shift in the object area occurs when the selected x_i changes, along with a shift of the horizontal fringes in the y direction, i.e. in the direction orthogonal to the object flow. On the other hand, a spatial shift of the object occurs in the flow direction, in turn resulting in a different mapping of the object on the *t* axis, so that the elements of Σ have to be realigned with respect to the *t* variable in order to be properly combined. Once realigned, three elements corresponding to separated rows of the linear sensor array are sufficient to implement a three step phase shifting algorithm [19-23]. The orthogonal shift of the fringes is used to estimate the minimum phase shift between adjacent pixel rows obtainable with the selected system parameters, namely the couple (p,γ), so that the elements of the stack providing the phase shift required result determined. Accordingly, selecting the triad

$$\{H_{si},H_{sj},H_{sk}\}=\{H_{s,\Delta\Psi=0},H_{s,\Delta\Psi=\pi/2},H_{s,\Delta\Psi=\pi}\}, \qquad (4)$$

where $\Delta\Psi$ is the phase shift, the complex object field can be directly recovered [43]. Supplementary Figure S1 resumes the processing steps required to synthesize the whole complex object field E(y,t) from three synthetic interferograms. Once the object field E(y,t) is estimated, numerical propagation allows flexible refocusing.

Experiments

The experimental set-up is a Mach-Zehnder interferometer as reported in Fig. 1. A laser beam at 632nm wavelength is firstly split in two parts, constituting the object beam and the reference beam respectively. The former passes through a portion of the microfluidic channel, where the samples flow at velocity *v* along the *x* direction and recombines with the reference to produce a fringe system in the acquisition plane (x,y). The produced interference pattern is recorded by a compact Linear Sensor Array (LSA) with (M,L)=(1024,64) square pixel which pitch is Δx=Δy=5.5μm. A Fourier configuration for the interferometer has been adopted, assuring straight and parallel fringes on the recording plane, inclined of an angle θ with respect to the *x* axis. The proposed method is conceived to be adopted in all the cases where uncontrolled mechanical rotations of the sample does not occur, as these would introduce object distortions in the synthetic image. On the other hand, a novel technique has been recently proposed which allows to avoid mechanical rotations without anesthetizing the live samples by trapping them inside Pluronic hydrogel droplets. Such droplets can then be brought back to the liquid phase by cooling a specific region of the chip, thus releasing the specimens [44].

Our purpose is to show that an interferogram as well as a hologram with unlimited FoV in the flow direction can be mapped in the space-time domain if the object movement is exploited. At this purpose, we acquired time sequences of interferograms with the LSA, resulting in a very narrow FoV along the *x* axis, because of the LSA dimensions (352 micron) in this direction. In a first experiment, we injected fibroblast cells, i.e. pure phase objects, and we let them flow along the channel using a remote controlled pump. Supplementary Movie 1 and Fig. 2 show the synthesis process of a space-time interferogram obtained with a single pixel row of the detector (which position is marked with a red solid line in Supplementary Movie 1 and fig. 2(a)). In this experiment, the limited ROI selected with the LSA allowed us to achieve higher frame rate, thus enabling to capture fast dynamics. It is worth to underline that, in order to obtain an undistorted image, a proper matching between the fluid speed and the acquisition frame rate has to be fulfilled, so that for an established acquisition frame rate F_R, only the object flowing with a velocity $v=F_R\Delta x$ will be correctly sampled in the synthetic hologram. Faster objects will be undersampled and appear squeezed in the synthetic hologram while slower objects will be oversampled and look like stretched. In the reported sequence, the cells were pushed by an air bubble formed inside the channel. The ensemble effect is not appreciable in the limited FoV (x,y) interferograms (see the sequence in Fig. 2(a)), while it is clearly shown in the corresponding (y,t) synthesis of Fig. 2(b) (in Fig. 2 we denoted with t_i, i=1,…,K, the dimensionless temporal coordinate after accounting for the frame rate of acquisition). As expected, the whole complex object information modulates horizontal fringes in the synthetic interferogram, from which a number of cells are visible inside the extended FoV as a result of their passage through the detection gate. Noteworthy, as an effect of the bubble pushing the fibroblasts, these cells experience an acceleration in the x direction, so that the requirement for a constant velocity and the matching between v and the frame rate is not fulfilled. This is apparent in Fig. 2(b) where a deformation of circular cells occurs and the most accelerated cells get severely undersampled. Although this is a drawback of the μSTSI method,

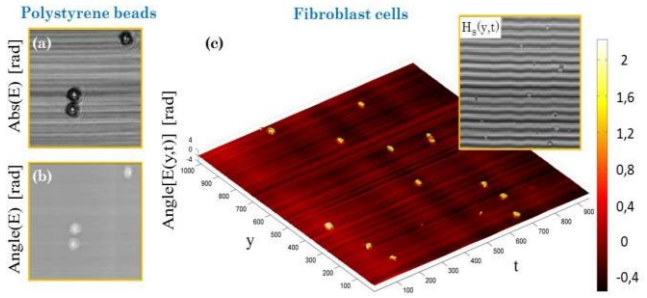

Fig. 3 Full-field recovery by PS-μSTSI. Experiments carried out using different test samples show the retrieval of the whole complex object field after applying a PS-μSTSI technique (see also Supplementary Movie 2 and Supplementary Figure S1). (a) Amplitude reconstruction and (b) phase-contrast map of polystyrene beads. (c) High throughput phase-contrast imaging of fibroblast cells flowing at constant velocity is shown, along with the corresponding extended FoV synthetic interferogram (in the inset).

it also allows to recover information about the objects dynamics (e.g. for speed-based sorting purposes) looking at a single synthetic image. In other words, relying on prior assumptions on the object shape, a synthetic reconstruction could automatically discard all the stretched objects, i.e. the one flowing with velocity lower than the selected speed, as well as the squeezed samples, i.e. the one moving with velocity higher than the threshold speed. In this way, from one recorded sequence, multiple maps could be provided as an output, augmenting the information throughput of the optofluidic system. Besides, the FoV is only limited in the y direction, while the acquisition of a longer time sequence assures a theoretically unlimited FoV along the *x* coordinate, allowing to capture information from more and more objects flowing inside the chip. If the diversity between three properly selected space-time interferograms is exploited, the presence of interference fringes allows the direct synthesis of the whole complex object field, E(y,t) by a PS algorithm. The processing steps are resumed in the block diagram shown in Supplementary Figure S1. As test samples, polystyrene beads were let flow along the microfluidic channel at constant velocity and captured by the LSA. Synthetic interferograms are built up according to Eq. (4), which are shown in Supplementary Figure S1(a). These are realigned along the t axis in order to be properly combined by means of a 3-step PS algorithm [43]. The final object amplitude reconstruction and the phase-contrast map, extracted from the estimated field E(y,t) are respectively shown in Fig. 3(a) and Fig. 3(b).

Hence, PS-μSTSI yields quantitative, extended FoV phase-contrast maps which are useful in all cases where multiple objects flow inside the chip. As a further example, Figure 3(c) shows a phase-contrast image of multiple fibroblast cells captured by the LSA (see Supplementary Movie 2) while flowing at constant velocity along the channel (the corresponding synthetic interferogram, $H_S(y,t)$, is shown in the inset of Fig. 3(c)).

In a second set of experiments, we studied biological samples of higher interest for biomedical investigations, namely *Caenorhabditis elegans* worms (details about the sample preparation can be found in the Supporting Information and in ref. [45]). *C.elegans* is an important model organism used to understand biological diseases. There are several features that make *C.elegans* an attractive model system for diverse biological approaches and applications. In particular the fully sequenced genome [46], its simplified nervous system and body transparency, that offers the advantage of visualizing individual neurons, in living worms, while the processes take place; the complete characterization of cell lineage, which is largely invariant between individuals; a small number of cells (959 in the adult hermaphrodite) and neurons (302 in the adult) and the possibility to easily genetically manipulate it without many ethical concerns. All these features have paved the way for the choice of *C.elegans* as organism for neurobiology, toxicology, ecology, developmental biology and molecular biology studies [47,48]. The conservation of proteins and pathways between nematodes and humans, with more than 70% of disease genes presenting a nematode orthologue lead to the successfully reproduction, in *C.elegans* of a wide number of human diseases such as metabolic and neurological disorders as Parkinson's and Huntington's [49,50]. These disease relevant models have been used also in high throughput screenings in order to find chemical compounds and to identify gene targets and cellular processes mostly controlling the disease related phenotypes [51,52]. As pointed-out before, in standard imaging, a trade-off exists between the obtainable FoV and the magnification, so that a poor magnification and, in turn, spatial resolution, is achievable when the whole sample interferogram has to be captured in a single shot. This is very important with multicellular organisms, such as *C.elegans* that, measuring 1 mm in length as adult, is compatible with microfluidics but can hardly be imaged as whole-organism. Our purpose is to demonstrate here that such constraint can be overcome, as the μSTSI method provides interferograms as well as Digital Holograms with unlimited FoV in the flow direction, so that the desired magnification can be set and the spatial resolution is only bounded by the diffraction limit. We let *C. elegans* flow along the channel and we performed in-focus recordings with the LSA, as sketched in Fig. 4(a). In this experiment a low magnification (M=10) was set, so that a limited FoV was sufficient to show the whole object. In Figure 4(b) we reported one of the space-time interferograms obtainable with the

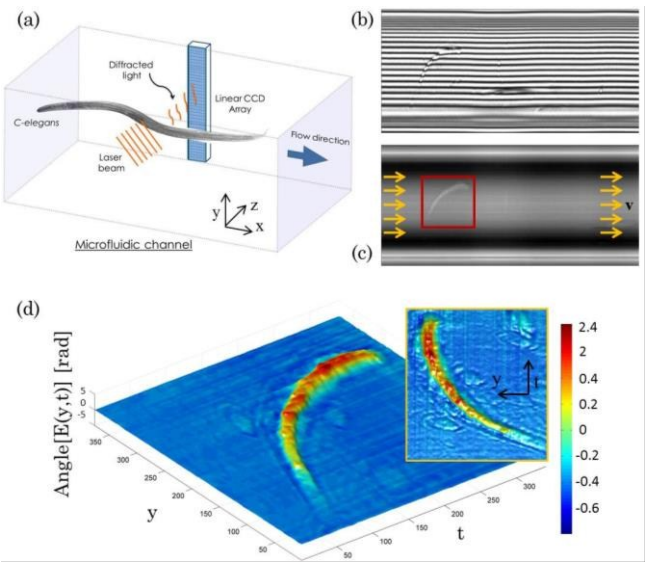

Fig. 4 The phase-contrast map of a *C-elegans* is estimated by PS-μSTSI. (a) A sketch of the experiment. (b) Synthetic interferogram. (c-d) Phase maps obtained before (c) and after (d) compensating the curvature due to the channel shape (see also Supplementary Figure S2 for details).

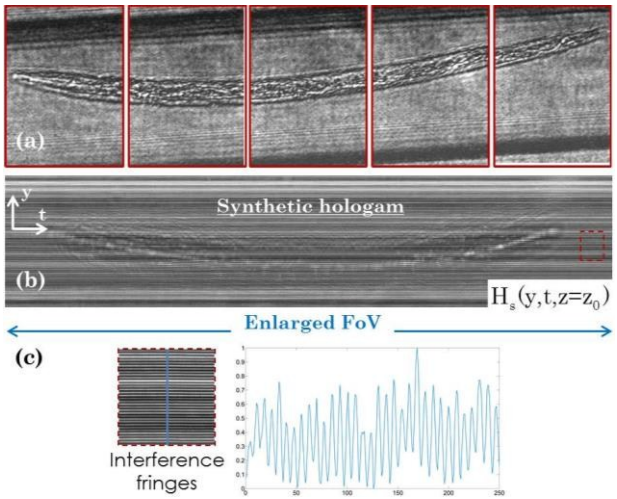

Fig. 5 Synthesis of a STDH. A C-elegans is imaged with high magnification (M=50) while flowing along the channel. (a) Time sequence of limited FoV optical images showing small portions of the sample, recorded in focus by a 2048x2048 CCD sensor for comparison. (b) STDH: a large FoV synthetic hologram is built up from out-of-focus recordings by a single line detector, carrying 3D information from the whole sample at a glance. (c) An inset shows the interference fringes along a line orthogonal to the flow direction

LSA, showing the flowing specimen while sampled by horizontal interference fringes. The corresponding space-time phase-contrast maps obtained with a 3-step PS algorithm are shown in Fig. 4(c) and Fig. 4(d), respectively reporting the unwrapped phase signal [53] before and after compensating the curvature due to the channel shape (see Supplementary Figure S2 for details).

Then, a different set of acquisitions has been performed with the aim to demonstrate that just one single detector array is sufficient to provide all the information necessary to build up a new type of digital hologram, namely a Space-Time Digital Hologram (STDH) with the following remarkable features:

- Independently of the fringe orientation on the acquisition plane, the space-time hologram shows horizontal fringes, i.e. parallel to the flow direction.
- Independently of the magnification and the FoV of the acquired (x,y) hologram, a space-time hologram has unlimited FoV along the flow direction, only depending on the overall acquisition time T, and obtainable without any complex hologram stitching procedure.
- A so built space-time hologram still maintains all the advantageous capabilities of DH, i.e. the possibility to achieve quantitative phase-contrast mapping in the plane (y,t) and, above all, flexible refocusing by numerical propagation along the optical axis, z. In other words, once the set of vectors $\mathbf{h}_1$, $\mathbf{h}_2$,…, $\mathbf{h}_K$ is acquired with a single line detector, it is possible to fill the whole stack couple:

$$A(y,t,z)=\left|P_z\left[H_s(y,t,z=z_0)\right]\right|$$
$$\phi(y,t,z)=\mathrm{Angle}\left\{P_z\left[H_s(y,t,z=z_0)\right]\right\}, \quad (5)$$

where $P_z(\ldots)$ denotes the propagation transform, $A(\ldots)$ is the object amplitude and $\phi(\ldots)$ is the phase contrast between the specimen and the medium.

- Differently from the case of PS-μSTSI, the whole complex object field is achievable with no need for image co-registration.
- Thanks to the movement of the objects along the microfluidic channel, it is easy to build up a reference synthetic hologram, selecting a temporal range in which no objects overcome the detection gate. This allows to directly estimate the object optical thickness, inherently compensating the phase contributions due to the optical elements along the object beam path (e.g. lens aberrations) and/or the curvature due to the channel shape. For the sake of simplicity, we will hereafter denote with $\phi(\ldots)$ the estimated phase signal after compensating the reference STDH.

In a STDH system the imaging time is the time the whole object takes to flow below the LSA. Hence, it depends on the object dimension in the x direction and its speed. The achievable resolution is mainly limited, as in common DH acquisition systems, by the sensor pixel dimensions (Δx,Δy) unless sub-pixel shifting of the object is exploited to apply a pixel super resolution algorithm [40-42]. As previously mentioned, the FoV is different along the two axis orthogonal to the optical one. Indeed, in the flow direction, x, this is proportional to the overall acquisition time, thus being theoretically unlimited. As in classical DH, the FoV along the y axis depends on the system parameters as $FoV_y=M\Delta y/M_y$, where M_y is the magnification in the y direction. If we consider the throughput of this imaging system as the time required to get an image representing the whole object, we found that this proportionally depends, for a fixed object size, on the object velocity and the frame rate. Since these are matched in our system ($v=F_R\Delta x$), the lower between them determines the maximum throughput. In other words, the throughput is not theoretically limited, but only depends on the adopted hardware, still taking advantage of the fact that a LSA can achieve higher frame rate with respect to a 2D sensor with comparable features.

In order to compare the results of the STDH synthesis and propagation process with expected ones, we performed captures of the specimen while this was flowing along the channel, illuminated with one optical beam and recorded in the sample best-focus plane by a common 2048x2048 CCD camera with $\Delta x=\Delta y=5.5\mu m$ pixel pitch. We selected images corresponding to a limited ROI (930x1260 pixels), each one showing a small part of the whole specimen (see Fig. 5(a)). Due to the sample length and the higher magnification we set (M=50), one single hologram would not be sufficient to capture the whole object, and a hologram stitching processing should be employed to provide a synthetic FoV enlargement. Indeed, it results $FoV_{CCD\_y}=FoV_{CCD\_x}=225{,}3\mu m$. Instead, here we performed out of focus recordings, setting closely spaced straight and parallel fringes, to proper code the specimen information. Fig. 5(b) illustrates the synthesis by one single raw detector of the STDH. For the sake of clarity, a zoom of the background area in the red dashed box of Fig. 5(b) is reported in Fig. 5(c) along with the interference fringes obtained selecting a line orthogonal to the flow direction. Given the system and the LSA parameters, it results $FoV_{LSA\_y}=FoV_{CCD\_y}=225{,}3\mu m$, while FoV_{LSA_x} is infinite. In this experiment, the FoV exploited along the x axis in order to capture the whole out-of-focus hologram of the sample was $FoV_{LSA\_x}=440\mu m$ (in STDH this parameter can be chosen as

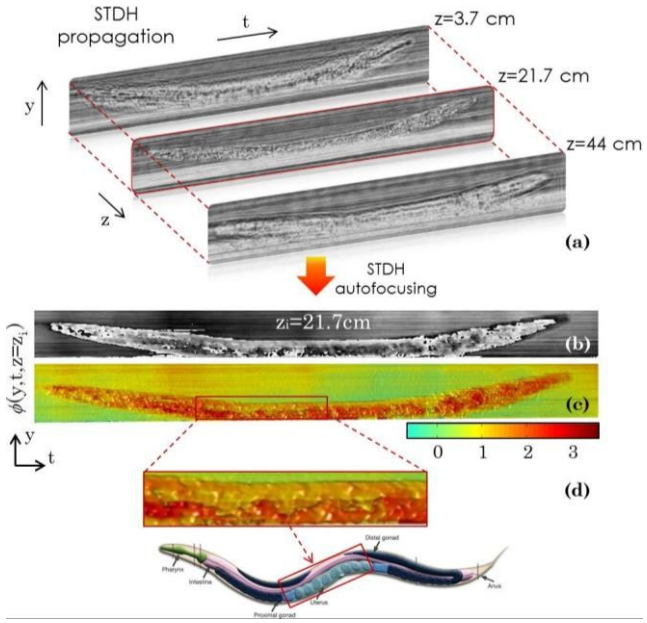

Fig. 6 STDH z-scanning and phase-contrast mapping after propagation at the sample best-focus distance, z_i =21.7cm. (a) Amplitude images extracted from the z-scanning stack are reported, showing the STDH automatic refocusing to estimate the sample best-focus distance (see Supplementary Movie 3 and Supplementary Figure S3). (b) Wrapped phase corresponding to the amplitude map in the red box in Fig. 6(a). (c) Unwrapped [53] phase [rad]. (d) An inset shows a detail of the object, where the areas with different optical thickness are recognizable and reveal the worm inner structure. The bottom part of Fig. 6(d) is reproduced from [55].

large as desired depending on the object size and M_x). We performed acquisitions with F_R=50Hz (v=5.5μm/s), so that the imaging time for this experiment was T=80s. For the sake of comparison, the previously reported Holographic Opto-fluidic Microscopy (HOM) method [40] yields lower imaging time (about 2-3s) for a CMOS full-field of 24mm^2, while the proposed STDH achieves a synthetic sensor dimension of 248mm^2 at the cost of a longer imaging time. However, the time required to get an hologram of the object is not lower bounded, and it could be drastically lowered adopting higher F_R and, in turn, higher sample velocity inside the channel.

Figure 5(b) corresponds to a blind recording where no prior information is exploited about the sample position inside the chip. However, according to Eq. (5), STDH propagation allows the z-scanning till reaching the sample best-focus plane. In Supplementary Figure S3 some significant amplitude reconstructions extracted from the stack A(y,t,z) are reported, showing the progressive image formation till focusing the sample at distance z=21,7cm and the subsequent defocusing in the image propagated at z=44cm. An automatic focusing algorithm based on a proper contrast estimator can be applied to the elements of A(y,t,z) to inspect all the planes in order to look for the sample best-focus distance [54]. In Fig. 6(b) and Fig. 6(c) we show the element ϕ(y,t,z=21.7cm), respectively before and after applying the phase unwrapping algorithm [53]. The inset of Fig. 6(d) shows areas with different optical thickness due to the inner structure of the specimen. The STDH propagation process, sketched in Fig. 6(a), is also presented in Supplementary Movie3. Thus, all the properties of STDH turn out to be proved.

Conclusions

The OFM shown in the 2006 represented a cutting-edge novelty in the field of optofluidic imaging for point-of-care diagnostics [30]. Since then, great effort has been spent to develop compact imaging systems suitable to be embedded onboard LoC platforms, with the aim to favor the spread of diagnostic tools of easy and rapid use. Among them, low-coherence flow-based scanning microscopes solve the problem of system compactness, but they cannot provide at the same time full-field imaging capabilities, high-throughput, wide FoV and magnification of the samples, as these are bounded to lensless, near-field diffraction based setups [15,31,40]. In particular, in all these techniques, the trade-off between resolution and FoV puts a hard bounding constraint to the throughput of the imaging system, while the need for a 2D sensor impairs to move a step toward the realization of compact chips with embedded imaging functionalities. Moreover, since the flowing objects occupy different positions along the optical axis, a best focus acquisition distance has to be chosen once. Without numerical post-propagation, a recording with un-coherent techniques cannot yield images where all the flowing objects are in focus, as the acquisition plane should be dynamically adjusted by mechanical z-scanning, which is unfeasible with fast flowing samples, further limiting the throughput. In this work, a novel coherent approach is presented which overcomes the above mentioned constraints, providing rapid, label-free, quantitative, flexible focusing, 3D imaging of samples flowing in LoC devices. A first example reported here shows the application to bio-microfluidics of the recently proposed STSI [43]. We have proved that it is possible to replace a 2D sensor with a 1D linear detector suitable to be embedded in a compact chip and achieving higher frame rate. In μSTSI, once the desired magnification of the sample is set, this only puts a FoV constraint in the normal direction to the flow. In other words, μSTSI achieves unlimited FoV along the sample flow and maintains all the advantageous features of PSI and scanning techniques, but with no cost associated with. Then, a new recording modality has been presented, leading to the synthesis of a new type of hologram (STDH) from a set of out-of focus recordings by a single line detector. The properties of the STDH have been shown, proving that re-focusable full complex fields can be yielded with unlimited FoV along the flow direction, with no need for hologram stitching. In other words, a so synthesized STDH possesses all the features of a common hologram built in a space-space domain, but assures high throughput. Hence, STDH looks a promising diagnostic tool for optofluidic investigations of biological specimens.

Acknowledgements

This work was supported by Progetto “Smart Cities” – Aquasystem: “Procedure e tecnologie innovative per una gestione pianificata ed integrata delle risorse idriche, l'ottimizzazione energetica ed il controllo della qualità nel Ciclo Integrato delle Acque”

Notes

[a]CNR-Istituto di Cibernetica "E. Caianiello",Via Campi Flegrei, 34, I-80078, Pozzuoli (NA), Italy.Fax: +390818675118; Tel: +390818675040; E-mail: melania.paturzo@cnr.it
[b]Institute of Biosciences and BioResources, IBBR-CNR, Via Pietro Castellino 111, 80131 Naples, Italy.
† Electronic Supplementary Information (ESI) available. See DOI: 10.1039/b000000x/

References

1 G. Cox, *Materials Today*, 2002, **5,** 34.
2 K. Dholakia and T. Čižmár, *Nat. Photonics*, 2011, **5**, 335.
3 S. Mavandadi, S. Feng, F. Yu, S. Dimitrov, K. N. Saines, W. R. Prescott and A. Ozcan, *Plos One*, 2012, **7**.
4 H. Zhu, S. O. Isikman, O. Mudanyali, A. Greenbaum and A. Ozcan, *Lab Chip*, 2013, **13**, 51.
5 H. C. Koydemir, Z. Gorocs, D. Tseng, B. Cortazar, S. Feng, R. Y. L. Chan, J. Burbano, E. McLeod and A. Ozcan, *Lab Chip*, 2014, Accepted Manuscript. DOI: 10.1039/C4LC01358A
6 E. McLeod, W. Luo, O. Mudanyali, A. Greenbaum and A. Ozcan, *Lab Chip*, 2013, **13**, 2028.
7 S. Monneret, F. Belloni and O. Soppera, *Microfluid. Nanofluid*, 2007, **3**, 645.
8 P. S. Dittrich and A. Manz, *Nat. Rev. Drug Discov*, 2006, **5**, 210.
9 F. Merola, L. Miccio, P. Memmolo, M. Paturzo, S. Grilli and P. Ferraro, *IEEE Phot. J.*, 2012, **4**, 451.
10 V. Bianco, F. Merola, L. Miccio, P. Memmolo, O. Gennari, M. Paturzo, P. A. Netti and P. Ferraro, *Lab Chip*, 2014, **14**, 2499.
11 A. Barroso, M. Woerdemann, A. Vollmer, G. von Bally, B. Kemper and C. Denz, *Small*, 2013, **9**, 885.
12 M. Padgett and R. di Leonardo, *Lab Chip*, 2011, **11**, 1196.
13 M. Kumara, N. Srividya, S. Muralidharan, and B. Tripp, *Nano Letters*, 2006, **6**, 2121.
14 Z. Göröcs and A. Ozcan, *IEEE Rev. Biomed. Eng*. 2013, **6**, 29.
15 A. Greenbaum, W. Luo, B. Khademhosseinieh, T. W. Su, A. F. Coskun and A. Ozcan, *Sci. Rep.*, 2013, **3**, 1717.
16 L. Miccio, P. Memmolo, F. Merola, S. Fusco, V. Embrione, A. Paciello, M. Ventre, P. A. Netti and P. Ferraro, *Lab Chip*, 2014, **14**, 1129.
17 Y. Cotte, F. Toy, P. Jourdain, N. Pavillon, D. Boss, P. Magistretti, P. Marquet and C. Depeursinge, *Nature Photon*, 2013, **7**, 113.
18 T. F. Wu, T. M. Yen, Y. Han, Y. J. Chiu, E. Y. Lin, Y. H. Lo, *Lab Chip*, 2014, **14**, 3341.
19 K. Creath, *Appl. Opt.*, 1985, **24**(18), 3053.
20 J. E. Greivenkamp, and J. H. Bruning, Phase shifting interferometry. Optical Shop Testing, 2nd ed., D. Malacara, ed. (Wiley, 1992), Chap. 14.
21 I. Yamaguchi and T. Zhang, *Opt. Lett.*, 1997, **22**(16), 1268.
22 J. P. Liu, and T. C. Poon, *Opt. Lett.*, 2009, **34**(3), 250.
23 I. Yamaguchi, J. Kato, S. Ohta and J. Mizuno, *Appl. Opt.*, 2001, **40**(34), 6177.
24 D Huang, E. A. Swanson, C. P. Lin, J. S. Schuman, W. G. Stinson, W. Chang, M. R. Hee, T. Flotte, K. Gregory, C. A. Puliafito, et. al., *Science*, 1991, **254**, 1178.
25 J. Sharpe, U. Ahlgren, P. Perry, B. Hill, A. Ross, J. H. Sørensen, R. Baldock, D. Davidson, *Science*, 2002, **296**, 541.
26 T. Kim, R. Zhou, M. Mir, S. D. Babacan, P. S. Carney, L. L. Goddard and G. Popescu, *Nature Photonics*, 2014, **8**, 256.
27 P. Memmolo, V. Bianco, F. Merola, L. Miccio, M. Paturzo and P. Ferraro, *IEEE Photon. J.*, 2014, **6**(2), 0701106.
28 F. Merola, P. Memmolo, L. Miccio, V. Bianco, M. Paturzo and P. Ferraro, *Proc. IEEE*, 2014. (Accepted manuscript). DOI: 10.1109/JPROC.2014.2375374
29 G. Zheng, R. Horstmeyer, and C. Yang, *Nat. Photonics*, 2013, **7**(9), 739.
30 X. Heng, D. Erickson, L. R. Baugh, Z. Yaqoob, P. W. Sternberg, D. Psaltis and C. Yang, *Lab Chip*, 2006, **6**, 1274.
31 D. W. E. Noom, D. E. B. Flaes, E. Labordus, K. S. E. Eikema, and S. Witte, *Opt. Exp.*, 2014, **22**(25), 30504.
32 R. Amézquita-Orozco, and Y. Mejía-Barbosa, *Opt. Exp.*, 2013, **21**(16), 19128.
33 C. H. Lu, N. C. Pégard, and J. W. Fleischer, *Appl. Phys. Lett.*, 2013, **102**, 161115.
34 N. C. Pégard, M. L. Toth, M. Driscoll, and J. W. Fleischer, Digital Holography and Three-Dimensional Imaging, 3D Imaging and Display Systems, Seattle, Washington, United States, July 13-17, 2014.
35 V. Micó, C. Ferreira, and J. García, *Opt. Exp.*, 2012, **20**(9), 9382.
36 J. H. Massig, *Opt. Lett.*, 2002, **27**(24), 2179.
37 J. Di, J. Zhao, H. Jiang, P. Zhang, Q. Fan and W. Sun, *Appl. Opt.*, 2008, **47**(30), 5654.
38 S. A. Alexandrov, T. R. Hillman, T. Gutzler and D. D. Sampson, *PRL, 2006*, **97**, 168102.
39 T. C. Poon, *J. Holography Speckle*, 2004, **1**, 6.
40 W. Bishara, H. Zhu and A. Ozcan, *Opt. Exp.*, 2010, **18**(26), 27499.
41 S. O. Isikman, W. Bishara, H. Zhu, A. Ozcan, *Appl. Phys. Lett.*, 2011, **98**(16), 161109.
42 S. C. Park, M. K. Park, M. G. Kang, *IEEE Signal Process. Mag.*, 2003, **20**(3), 21.
43 V. Bianco, M. Paturzo and P. Ferraro, *Opt. Exp.*, 2014, **22**(19), 22328.
44 G. Aubry, M. Zhana and H. Lu, *Lab Chip*, 2015, **15**, 1424.
45 S. Brenner, Genetics, 1974, **77**(1), 71.
46 R. Baumeister and L. Ge, *Trends Biotechnol.*, 2002, **20**(4), 147. PMID: 11906745
47 E. Di Schiavi and D. Andrenacci, *Curr Genomics*, 2013, **14**(1), 2.
48 T. Kaletta and M. O. Hengartner, *Nature Reviews Drug Discovery*, 2006, **5**, 387.
49 E. Culetto and D. B. Sattelle, *Hum Mol Genet.*, 2000, **9**(6), 869.
50 B. Alberts, *Science*, 2010, **330**, 1724.
51 T. J. Van Ham, R. Breitling, M. A. Swertz and E. A. Nollen, *EMBO Mol Med.*, 2009, **1**(8-9), 360.
52 D. Teschendorf and C. D. Link, *Mol Neurodegener.*, 2009, **4**(38).
53 J. M. Bioucas-Dias and G. Valadão, *IEEE Trans. Image Process.*, 2007, **16**(3), 698.
54 P. Memmolo, M. Paturzo, B. Javidi, P. A. Netti and P. Ferraro, *Opt. Lett.*, 2014, **39**, 4719.
55 www.wormatlas.org